Title
Measurement of tissue absorption coefficients by use of interferometric photothermal spectroscopy.

Journal
Applied Optics, 38(7)

ISSN
0003-6935

Authors
Yablon, AD
Nishioka, NS
Mikić, BB
et al.

Publication Date
1999-03-01

DOI
10.1364/ao.38.001259

Measurement of tissue absorption coefficients by use of interferometric photothermal spectroscopy

Andrew D. Yablon, Norman S. Nishioka, Bora B. Mikić, and Vasan Venugopalan

We describe a spectroscopic technique called interferometric photothermal spectroscopy (IPTS) that can measure the absorption coefficient of pulsed laser radiation in nonscattering tissue samples. The technique is suitable for measuring effective absorption coefficients from 10^3 to 10^5 cm^{-1}. IPTS is particularly attractive because it requires minimal disturbance of the sample. These features indicate potential use for *in vivo* measurements of tissue absorption coefficients. To validate the technique, the absorption coefficient of pulsed *Q*-switched Er:YSGG (2.79-μm) radiation in pure water was measured to be 5200 (±500) cm^{-1} when IPTS was used, in agreement with other published values. IPTS was also used to measure the absorption coefficient of pulsed ArF excimer laser radiation (193 nm) in bovine corneal stroma (*in vitro*), giving a value of 1.9 (±0.4) × 10^4 cm^{-1}. © 1999 Optical Society of America

OCIS codes: 120.3180, 120.4290, 120.6810, 170.3660, 170.6930, 300.6430.

1. Introduction

There is strong interest within the medical community in developing minimally invasive techniques for probing living tissue. The thermal response of tissue to pulsed laser irradiation can be used to obtain information about tissue thermophysical properties and structure. An example of this is pulsed photothermal radiometry in which the radiative emission from a tissue sample heated by a laser pulse is used to infer the depth, location, and absorption of tissue chromophores.[1,2] We have developed a novel technique called interferometric photothermal spectroscopy (IPTS) for measuring the absorption coefficient of pulsed laser radiation in nonturbid tissue samples or the effective absorption coefficient in turbid samples. In IPTS an interferometer is used to measure surface displacement resulting from thermal expansion induced by a pump laser pulse. This interferometer is similar to an instrument developed by Albagli and co-workers[3,4] but has a lower noise floor and a faster rise time. An analytic model of the tissue thermal response was used to extract the absorption coefficient from the interferometer displacement trace. IPTS is not meant to replace traditional techniques such as transmission spectroscopy but rather to complement them and permit measurements of the tissue absorption coefficient that might otherwise be impossible.

The thermal response of an irradiated target is a powerful method for estimating the characteristic optical absorption depth of pulsed radiation in tissue because the time required for thermal energy to diffuse out of a heated volume varies with the square of the volume's smallest dimension. If the transverse width of the laser beam is much larger than the penetration depth in the tissue, the time required for thermal energy to diffuse away will scale with the square of the penetration depth. Thus the time scale for thermal relaxation is a sensitive indicator of optical absorption characteristics.

Figure 1 shows the IPTS technique schematically. The pulse energy of the pump laser must be delivered in conditions of thermal confinement and requires the laser pulse duration to be much shorter than the characteristic time necessary for thermal energy to diffuse out of the irradiated volume. The thermal energy imparted to the tissue by the laser pulse results in thermal expansion and motion of the tissue surface. Subsequent thermal diffusion leads to further surface motion provided that either the expansion properties of the material are variable with

A. D. Yablon and N. S. Nishioka are with the Wellman Laboratories of Photomedicine, Massachusetts General Hospital, Boston, Massachusetts 02114. B. B. Mikić is with the Department of Mechanical Engineering, Massachusetts Institute of Technology, Cambridge, Massachusetts 02139. V. Venugopalan (vasan@bli.uci.edu) is with the Laser Microbeam and Medical Program, Beckman Laser Institute, 1002 Health Sciences Road, University of California, Irvine, Irvine, California 92612.

Received 30 June 1998; revised manuscript received 9 November 1998.

0003-6935/99/071259-14$15.00/0

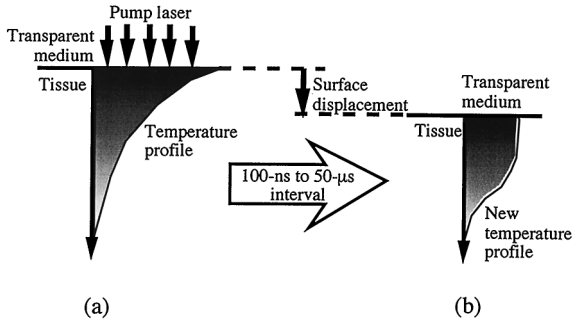

Fig. 1. IPTS technique: (a) Laser energy has been completely deposited and no thermal diffusion has occurred although thermal stresses have equilibrated. An interval of approximately 100 ns to 50 μs transpires between (a) and (b). (b) Thermal diffusion has resulted in detectable surface displacement whose time scale and magnitude yield an effective penetration depth.

temperature or a significant amount of energy is permitted to escape through the target surface. The latter can be achieved by placement of a thermally conductive but optically transparent material in contact with the sample. It is this subsequent surface displacement due to thermal diffusion that IPTS employs to determine the absorption or effective attenuation coefficient.

In practice, the range of absorption coefficients measurable by IPTS on a tissue target is limited. With our instrumentation the IPTS technique can be used effectively to measure absorption coefficients in the range of 10^3–10^5 cm^{-1} provided that the thermal and the acoustic properties of the tissue are similar to water. Weaker absorption results in longer thermal relaxation times (>50 μs), and the effect of ambient acoustic surface waves on the sample corrupts the surface-displacement signal. The ambient acoustic waves may result from acoustic noise in the environment. For larger absorption coefficients the magnitude and the time scale of the thermal relaxation will exceed the resolution (~1 nm) and the bandwidth limits (~4 ns) of the present interferometer.

For IPTS to be effective a significant temperature rise (a maximum of ~30°–80 °C) must be created in the tissue sample. Depending on the laser pulse parameters and tissue properties, this high temperature may persist for a few microseconds, and consequently the tissue might sustain some thermal damage. Since the tissue temperature during IPTS may approach, and in some cases exceed, 100 °C, an impermeable membrane is often required to seal the tissue surface and prevent vaporization that would otherwise corrupt the displacement signal obtained by the interferometer.

Albagli and co-workers[3–5] have suggested that thermoelastic surface displacement resulting from equilibration of thermal stresses induced by inertially confined laser irradiation can be used to measure the tissue absorption coefficient. Inertially confined irradiation is achieved when the laser pulse duration is shorter than the time required for an acoustic wave to traverse the heated tissue volume and results in no significant motion of the tissue on the time scale of the laser pulse. The time scale of the tissue surface motion is governed by the acoustic-wave velocity and the optical penetration depth of the heating laser pulse. However, to our knowledge, this technique has not yet been employed to measure an unknown absorption coefficient. One potential problem with this technique is that the induced thermal stresses may cause tissue mechanical damage. In tissue the thermal diffusion time greatly exceeds the mechanical equilibration time. Thus, for satisfying the instrumentation bandwidth constraints (defined by the interferometer rise time and ambient surface acoustic waves), a technique predicated on thermal stress equilibration is better suited to measuring small absorption coefficients (penetration depths of ~10 μm to 1 mm), while a thermal technique such as IPTS is better suited to measuring larger absorption coefficients (penetration depths of ~250 nm to 10 μm).

In this paper we formulate the theoretical basis for IPTS and demonstrate its use in measuring the optical absorption coefficient of pure water and *in vitro* samples of bovine corneal stroma. Both targets exhibit minimal optical scattering at the wavelengths tested. Experiments were performed on pure water to demonstrate the validity and the effectiveness of the IPTS technique, because the thermal, the mechanical, and the optical properties of water are well known. The *Q*-switched Er:YSGG laser (λ = 2.79 μm) served as the pump laser for the experiments with pure water because thermal modeling is simplified when the target material exhibits linear absorption of laser energy. Investigators have documented that pure water is a linear absorber at 2.79 μm provided the volumetric energy density imparted to the water is less than 3000 kJ/m^3.[6,7] In addition the 50-ns *Q*-switched Er:YSGG laser pulse energy provides thermally confined heating in pure water.

IPTS was also employed to measure the absorption coefficient of pulsed ArF excimer laser radiation (193 nm) in the cornea since it is not well characterized[8–14] and is important for understanding the dynamics of 193-nm corneal ablation employed for laser photorefractive keratectomy. The cornea is a transparent laminar structure approximately 600 μm thick that is the outer covering for the front of the eye. Since photorefractive keratectomy is primarily concerned with ablation of the corneal stroma, the goal of this experiment was to measure the absorption coefficient μ_a for this tissue.

2. Theoretical Modeling

In this section a derivation of the thermoelastic model employed for determining the absorption coefficient is presented. We begin by deriving the time evolution of the temperature field in the irradiated sample and then discuss how the thermal field influences the target surface displacement.

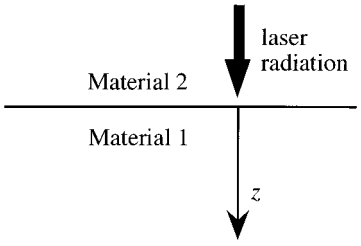

Fig. 2. Geometry for derivation of the IPTS model. Material 1 is the target material (tissue), which is a thermally semi-infinite body. Material 2 (saran, glass, or air) is transparent to the incident pumping laser pulse.

A. Thermal Field

As indicated in Fig. 2 the target tissue is termed material 1 and modeled as a semi-infinite body with axial coordinate z. Coupled to it is another semi-infinite body (i.e., air, saran, or glass) termed material 2, which is transparent to the incident laser radiation. The initial target temperature and density are spatially uniform and defined as T_0 and ρ_0, respectively. A laser pulse of short duration heats the target material. For linear absorption the volumetric energy deposition profile decays exponentially with a decay constant of D (effective penetration depth) in length units or μ_a (absorption coefficient) in inverse length units. The heating will be one dimensional (purely a function of z) provided that $D \ll w$, where w is the characteristic transverse width of the pump laser beam. This heating results in a temperature field that varies with time and space and is denoted by $T(z, t)$. Dilatation of the target material resulting from thermal expansion is assumed not to affect the temperature field or its time evolution.

The temperature field in both semi-infinite bodies is governed by heat conduction. Other energy transport modes such as convection and radiation are considered to be negligible. Convection is ignored owing to small spatial scales and the symmetry of the problem. Moreover the structural matrix of tissue is likely to suppress any bulk flow. Radiation is ignored because the temperature differences that we consider are small (<100 °C). We assume that the spatial scale of the heating is less than the thermal emission wavelength ($D < \lambda_{\text{thermal}}$), so the heated target is in the thin optical limit in which thermal emission is suppressed.[15]

Material 1 has a temperature field $T_1(z, t)$ with constant thermal conductivity k_1 and constant thermal diffusivity α_1. Likewise material 2 has a temperature field $T_2(z, t)$ with constant thermal conductivity k_2 and thermal diffusivity α_2. No volumetric heat sources are included in this model; rather the laser irradiation is modeled as an initial temperature distribution in the lower target material. This gives a solution valid for $t > \tau_p$, where τ_p is the laser pulse duration providing the laser energy is thermally confined, i.e., $D \ll (\alpha_1 \tau_p)^{1/2}$, so that negligible conduction occurs during the laser pulse.

The problem may be formally posed in terms of the governing equations and their associated boundary conditions. To simplify the derivation, we define $\theta(z, t) \equiv T - T_0$, where T_0 is the ambient temperature. The conduction equations for both materials may be written as

$$\frac{\partial \theta_1}{\partial t} = \alpha_1 \frac{\partial^2 \theta_1}{\partial z^2}, \qquad \frac{\partial \theta_2}{\partial t} = \alpha_2 \frac{\partial^2 \theta_2}{\partial z^2}. \tag{1}$$

The boundary conditions are

$$\begin{aligned} \theta_1(z = 0, t) &= \theta_2(z = 0, t), \\ k_1 \frac{\partial \theta_1(z = 0, t)}{\partial z} &= k_2 \frac{\partial \theta_2(z = 0, t)}{\partial z}, \\ \theta_1(z = \infty, t) &= 0, \\ \theta_2(z = -\infty, t) &= 0. \end{aligned} \tag{2}$$

Finally, we consider the case of a purely absorbing medium for which the initial condition in material 1 is

$$\theta_1(z, t = 0) = \frac{\mu_a \phi_0}{\rho_{0,1} c_{p,1}} \exp(-\mu_a z), \tag{3}$$

where ϕ_0 is the radiant exposure crossing the surface of material 1, $\rho_{0,1}$ is the density of material 1 at ambient temperature, and $c_{p,1}$ is the isobaric specific heat of material 1.

Equations (1) are solved by the method of Laplace transforms with the boundary conditions of Eqs. (2) and the initial condition of Eq. (3) to yield the temperature distribution for both regions:

$$\begin{aligned} \theta_1(z, t) = \frac{\mu_a \phi_0}{2\rho_{0,1} c_{p,1}} \exp(\mu_a{}^2 \alpha_1 t) \Bigg(& \exp(-\mu_a z) \\ & \times \left\{ 2 - \operatorname{erfc}\left[\frac{z}{2(\alpha_1 t)^{1/2}} - \mu_a (\alpha_1 t)^{1/2} \right] \right\} \\ & + \left[\frac{k_1 - (\alpha_1/\alpha_2)^{1/2} k_2}{k_1 + (\alpha_1/\alpha_2)^{1/2} k_2} \right] \exp(\mu_a z) \\ & \times \operatorname{erfc}\left[\frac{z}{2(\alpha_1 t)^{1/2}} + \mu_a (\alpha_1 t)^{1/2} \right] \Bigg), \end{aligned} \tag{4}$$

$$\begin{aligned} \theta_2(z, t) = & \frac{k_1}{k_1 + k_2 \left(\frac{\alpha_1}{\alpha_2} \right)^{1/2}} \frac{\mu_a \phi_0}{\rho_{0,1} c_{p,1}} \\ & \times \operatorname{erfc}\left[\mu_a (\alpha_1 t)^{1/2} - \frac{z}{2(\alpha_1 t)^{1/2}} \right] \\ & \times \exp\left[\mu_a{}^2 \alpha_1 t - \mu_a z \left(\frac{\alpha_1}{\alpha_2} \right)^{1/2} \right]. \end{aligned} \tag{5}$$

The accuracy of these solutions was verified with the aid of a finite-element-method (FEM) software package (MATLAB, The Mathworks, Natick, Mass.). Sample temperature profiles obtained from Eqs. (4) and (5) are depicted in Fig. 3.

According to this model the temperature increase in material 2 arises solely from energy that diffuses across the boundary from material 1. The cumulative energy transferred from material 1 to material 2 across the plane $z = 0$ at time t, $Q_{1\to2}(t)$, can be expressed as

$$Q_{1\to2}(t) = \int_0^t k_2 \frac{\partial\theta_2(z=0,t)}{\partial z}\,dt = \frac{\alpha_1 k_2 \phi_0}{k_1(\alpha_1\alpha_2)^{1/2} + \alpha_1 k_2} \times \{1 - \exp(\alpha_1\mu_a{}^2 t)\mathrm{erfc}[\mu_a(\alpha_1 t)^{1/2}]\}. \quad (6)$$

B. Surface Displacement

The dynamics of the thermal field produce a transient surface displacement in material 1 because of thermal expansion. In Appendix A we derive Eq. (7) for the net thermal expansion of material 1, $\Delta z(t)$, assuming that the thermal stresses have equilibrated, material 1 is isotropic, incompressible (Poisson's ratio is 0.5), and the entire expansion occurs in the z direction owing to one-dimensional heating:

$$\Delta z(t) = \int_0^\infty \left\{\frac{\rho_0}{\rho[T(z_0,t)]} - 1\right\} dz_0. \quad (7)$$

Note that we have not established precisely where the net expansion occurs, for it may not manifest itself as a displacement of the interface between the two materials. This issue is addressed below.

The computation of Eq. (7) requires knowledge of the temperature dependence of ρ. In general this is not known for tissue but is well characterized for water, the main constituent of soft tissue. In many cases the water content of soft tissue is large enough that the thermophysical properties of pure water are a sufficient approximation to those of tissue. Equation (8) is an accurate representation of the temperature dependence of the density of liquid water, where ρ_{water} is given in kilograms per cubic centimeter and T in degrees Celsius.[16] It is valid for water from 0 to 150 °C at atmospheric pressure (for 100 °C $< T \le$ 150 °C the water is in a metastable state):

$$\rho_{\mathrm{water}}(T) = \frac{999.8 + 16.95T - 7.987\times10^{-3}T^2 - 46.17\times10^{-6}T^3 + 105.6\times10^{-9}T^4 - 280.5\times10^{-12}T^5}{1 + 16.88\times10^{-3}T}. \quad (8)$$

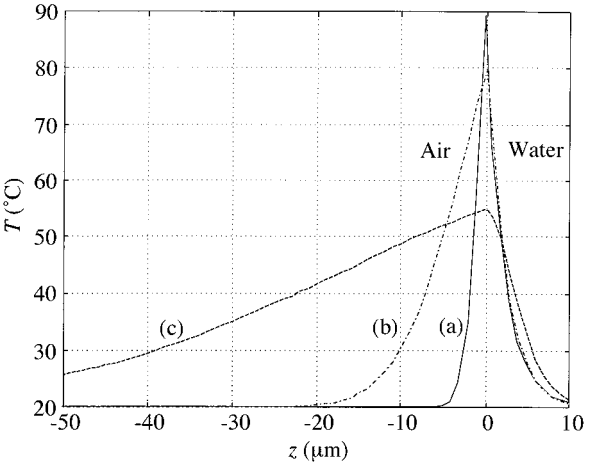

Fig. 3. Equations (3) and (4) plotted for a 650-J/m^2 pulse Er:YSGG laser pulse with μ_a = 4610 cm^{-1}. Material 1 is water, material 2 is air, and ambient temperature is 20 °C. The three traces correspond to (a) 50 ns, (b) 1 μs, and (c) 20 μs after the laser pulse.

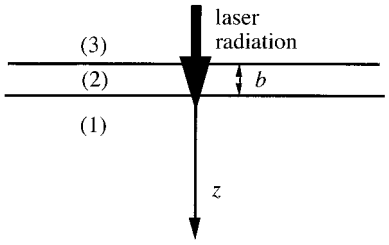

Fig. 4. Acoustically thin layer: (1) Semi-infinite target, material 1 (tissue); (2) acoustically thin layer (saran or glass) assumed to be transparent to the incident laser pulse with thickness b; (3) upper semi-infinite body (air) also assumed to be transparent to the incident laser pulse.

The interferometer employed in this study monitors the displacement of an interface. Thus we must determine how the transient displacement given by Eq. (7) maps to the displacement of the interface being monitored. This requires consideration of acoustic-wave propagation in the system. The acoustic impedance Z of materials 1 and 2 determines the displacement of the interface. The acoustic impedance is a material property defined as $Z = \rho c_a$, where c_a is the sonic velocity in the material. When $Z_1 \gg Z_2$ the interface is a free surface and material 2 offers negligible resistance to the motion of material 1. Thus the full extent of the thermal expansion predicted by Eq. (7) results in an upward displacement of the interface. This behavior occurs for water or tissue expanding into air ($Z_{\mathrm{water}} = 1.49\times10^6$ kg/m^2 s, $Z_{\mathrm{air}} = 393$ kg/m^2 s).

In the experiments an impermeable barrier is placed on top of the sample whose optical properties are being measured. This is done to suppress vaporization when the target material is heated near 100 °C. For optimal performance of the IPTS technique, this barrier should have several properties: it should (a) be optically transparent to the pump laser radiation, (b) be acoustically thin, (c) possess a refractive index similar to tissue, and (d) be thermally thick.

Optical transparency of the barrier is beneficial because it provides maximum coupling of the pump laser energy to the target and minimizes thermal expansion of the barrier itself. As is shown in Fig. 4, the barrier is chosen to be acoustically thin so that it does not impede the expansion of material 1. This is achieved when the thickness of layer b is less than half of the wavelength of the acoustic disturbance λ_a, i.e., $b < \lambda_a/2$. For events during which mechanical confinement is not achieved, $\lambda_a = \tau_p c_a$, so that λ_a is simply the distance an acoustic disturbance can propagate during the laser irradiation. It is also good to have a barrier with a refractive index close to that of the tissue to minimize any reflections of either the pump or the probe beams at the interface between the barrier and the tissue. Finally, the barrier should be thermally thick, i.e., sufficiently thick that thermal energy cannot traverse its width during the time that we are monitoring the displacement, usually many microseconds. This permits the barrier to be modeled as a semi-infinite body and maximizes the thermal energy transfer from the target to the barrier. The energy transfer from the target (material 1) to the barrier (material 2) will cause the barrier to expand. For a barrier with a temperature-independent thermal-expansion coefficient, the net expansion of the barrier $\Delta z_2(t)$ is

$$\Delta z_2(t) = \alpha_{T,2} \frac{Q_{1\to 2}(t)}{\rho_2 c_{p,2}}, \tag{9}$$

where $\alpha_{T,2}$ is the thermal-expansion coefficient of the barrier and $Q_{1\to 2}(t)$ is given by Eq. (6). For the experiments reported here this expansion is small, amounting to less than 10% of the total expansion of the target material. The interface between air and the acoustically thin layer is usually the easiest interface to monitor because it usually has the largest refractive-index mismatch and thus the largest optical reflectivity. When the motion of this interface is considered, the thermal expansion of the barrier must be accounted for. Note that according to our sign convention Δz is positive for dilatation. Thus, if the interface moves in the positive z direction (i.e., downward), Δz will be negative.

3. Materials and Methods

A. Interferometer

The interferometer employed to monitor the surface displacement of the tissue is depicted in Fig. 5.[17] It is a modified Mach–Zehnder interferometer employing a linearly polarized He–Ne laser (Melles Griot, Irvine, Calif.) operating at 632.8 nm. The He–Ne beam passes through an acousto-optic modulator (AOM) (IntraAction Corporation, Bellwood, Ill.) that splits it into two beams and imparts a 110-MHz frequency shift to one of the beams. The unshifted beam serves as the sample arm of the interferometer and is imaged on the sample surface at normal incidence. As depicted in Fig. 5 the pump laser pulse must approach the target surface at a slight angle.

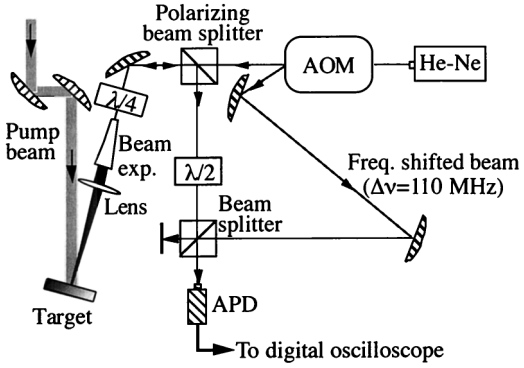

Fig. 5. Modified Mach–Zehnder interferometer employed to monitor target surface displacement resulting from a pump laser pulse. The AOM gives the reference arm of the interferometer a 110-MHz frequency shift and permits determination of the direction and the extent of the target surface displacement. In the sample arm of the interferometer the He–Ne beam was imaged onto the target surface with a beam expander and a 125-mm focal-length singlet lens. The half-wave plate ($\lambda/2$) and quarter-wave plate ($\lambda/4$) had their fast axes aligned at 45° to the plane of He–Ne polarization. As illustrated, the pump beam approached the sample at a slight angle to permit the He–Ne probe beam to interact with the target surface at normal incidence. The interference fringes detected by the APD were sampled by a digital scope and demodulated to reveal the surface displacement of the tissue target. This instrument had a 4-ns rise time and a noise floor of approximately 1 nm on pure water and bovine corneal stroma targets (not to scale).

The state of polarization of the He–Ne beam is manipulated to maximize the signal in the interferometer. In the sample arm the quarter-wave plate converts the linearly polarized beam into a circular polarization that then reflects off the sample surface. The reflected beam makes another trip through the quarter-wave plate and is converted to a linear polarization orthogonal to that of the original beam. This allows its separation from the original beam with the polarization-sensitive beam splitter. The half-wave plate is used to convert this orthogonal polarization into the original He–Ne polarization so that the reference and the sample beams may be interfered with.

The interference fringes are detected by a 250-MHz avalanche photodiode (APD) (EG&G, Quebec, Canada). Maximum fringe visibility occurs when the sample beam and the reference beam have equal intensities at the APD. The ratio of energy partitioned by the AOM into the sample and the reference beams is tuned for maximum fringe visibility, and this typically occurs when ~5% of the original He–Ne energy is directed into the reference arm and the remaining 95% is sent into the sample arm, because only a few percentage points of the incident light focused on the tissue surface are reflected back to the interferometer.

A 500-MHz, 1-Gs/s digital oscilloscope (Tektronix, Wilsonville, Ore.) samples both the photodiode signal and the rf signal driving the AOM. Both traces are acquired and processed by a PC (Apple Computer, Cupertino, Calif.). An application written in Lab-

View (National Instruments, Austin, Tex.) compares the phase of the fringes with that of the AOM drive signal and calculates the target displacement as a function of time. The surface displacement is related to the fringes detected by the APD and the rf drive signal through

$$\Delta z(t) = \frac{\lambda}{2}\frac{[\Phi_{\mathrm{APD}}(t) - \Phi_{\mathrm{AOM}}(t)]}{2\pi}, \qquad (10)$$

where $\Delta z(t)$ is the time-dependent target surface displacement, λ is the He–Ne laser wavelength (632.8 nm), $\Phi_{\mathrm{APD}}(t)$ is the time-dependent instantaneous phase (in radians) of the sinusoidal fringes detected by the APD, and $\Phi_{\mathrm{AOM}}(t)$ is the time-dependent instantaneous phase of the sinusoidal AOM drive voltage. The LabView application determines the instantaneous phase from the digitally sampled signals with the aid of the Hilbert transform. The interferometer is capable of a 4-ns rise time and 1-nm displacement accuracy (corresponding to 0.02 rad of relative phase) on specular targets such as liquid water, saran film, or glass.[17]

B. *Q*-switched Er:YSGG Laser Irradiation of Water

To test the validity of the model presented in Subsection 3.A, we investigated the behavior of pure water irradiated by a 2.79-μm *Q*-switched Er:YSGG laser. For these experiments an acoustically thin impermeable barrier was necessary to prevent surface vaporization of the water. Ordinary Saran Wrap (Dow Brands) was found to be a suitable choice because it is highly impervious to water.[18] In previous experiments we confirmed that the saran film absorbs a negligible amount of the 2.79-μm radiation. For this case $\alpha_{\mathrm{water}} = 1.46 \times 10^{-7}$ m^2/s, $b = 12.7$ μm, $\tau_p = 50$ ns, $D \sim 2.1$ μm,[7,19] $c_{a,\mathrm{water}} \sim 1500$ m/s, $c_{a,\mathrm{saran}} \sim 592$ m/s.[18] From these parameters it is easy to show that the laser pulse energy is not mechanically confined but is thermally confined within the water substrate. One can also show that $(\lambda_a/2) \sim 15$ μm $> b$ so the saran membrane is acoustically thin and will not impede water expansion. For sufficiently short times following the laser pulse ($t \ll b^2/\alpha_{\mathrm{saran}}$), the thin saran film will behave as a semi-infinite body since the thermal energy imparted by the laser to the water substrate will not have had enough time to diffuse across the saran film. In that case the thermal field in the pure water substrate will be described by Eq. (4) whereas the thermal field in the saran layer will be described by Eq. (5).

Samples of pure, deionized, triple-distilled water were prepared in 7-ml scintillation vials (Fisher Scientific) and covered with saran film. The saran film was sealed onto the water samples with a heat gun to ensure a wrinkle-free, taut film. In a separate experiment we determined that the saran absorbed $<5\%$ of the incident 2.79-μm radiation by measuring the energy of a laser pulse both before and after a single layer of the film was traversed. An Er:YSGG laser (Schwartz, Model SEO 1-2-3) was *Q* switched with a mechanical rear cavity mirror. A diagram of the setup and the geometry is presented in Figs. 6 and 7.

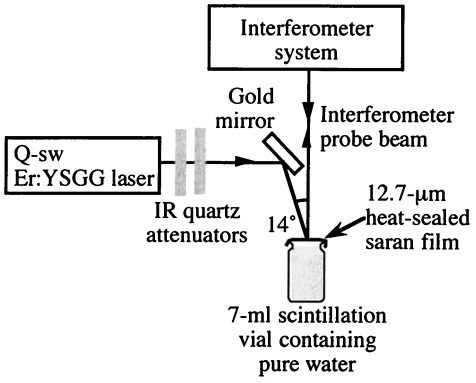

Fig. 6. Experimental setup for *Q*-switched Er:YSGG irradiation of saran-covered water samples (not to scale).

The interferometer probe beam was imaged onto the saran–air interface with a 125-mm focal-length lens at normal incidence. Because the He–Ne laser beam entering the lens was collimated and 10 mm across, the focal spot was $\sim$15 μm in diameter. The depth of focus of the focused He–Ne beam was $\sim$700 μm. The interferometer beam remained fixed during the experiment and, because of the very short depth of focus, defined a fixed zone in space where data were acquired. The heating of the water by the He–Ne probe beam was negligible owing to the small absorption and scattering of water and saran film at 632.8 nm. The heating of the tissue target and the saran film by the pump beam leads to a small change in their refractive indices but we neglected these effects.

The Er:YSGG pump laser beam was inclined at a 14° angle (in the air above) to the He–Ne laser beam to permit the He–Ne probe to approach the saran–water system at normal incidence. The refractive index of pure water at 2.79 μm is 1.315,[19] so the Er:YSGG laser radiation propagated at 10.6° to the

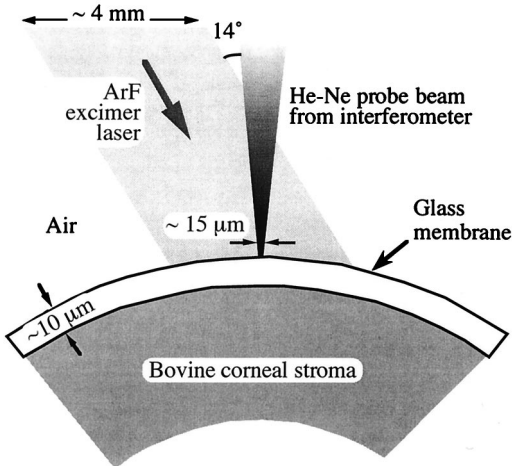

Fig. 7. Expanded view of Er:YSGG irradiation of saran-covered water samples (not to scale).

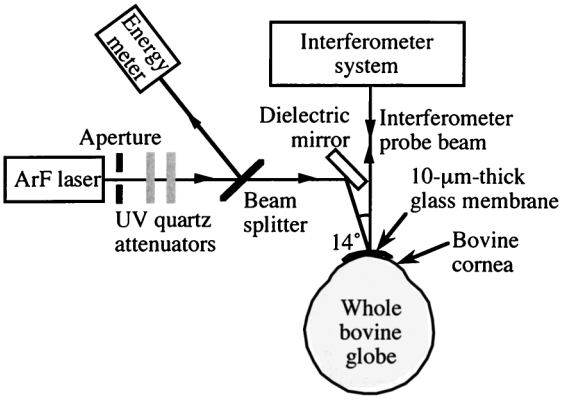

Fig. 8. Setup for ArF irradiation of bovine cornea (not to scale).

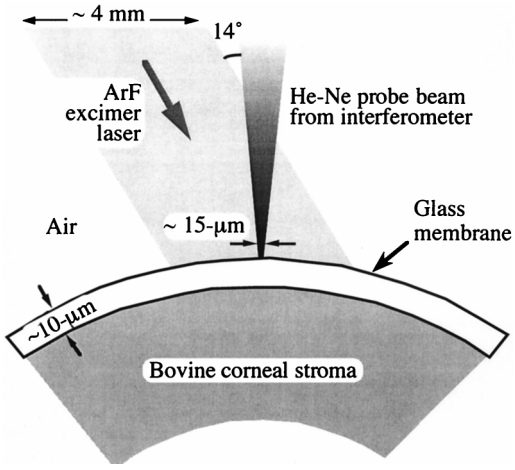

Fig. 9. Expanded view of setup for ArF excimer laser irradiation of bovine cornea (not to scale).

vertical within the water sample. Thus the measured absorption depth of the 2.79-μm radiation was cos(10.6°) of its actual value. We corrected for this small effect when presenting the results in Section 4. The term μ_a for 2.79-μm radiation in water is quoted as 4610 cm^{-1} (D = 2.17 μm) by Downing and Williams[19] and 5160 cm^{-1} (D = 1.94 μm) by Vodopyanov.[7]

The Er:YSGG laser system delivered 25-mJ pulses of 50-ns (FWHM) duration at a repetition rate of ~1 Hz with a transverse beam diameter of ~4 mm. The beam was aligned to be concentric with the interferometer probe beam on the saran film surface with the aid of gold mirrors. Unfortunately the mechanical Q-switching mechanism employed in the Er:YSGG laser resulted in significant shot-to-shot variation in both the spatial mode shape and the pulse energy. Since a laser beam analyzer was not available, it was not possible to measure accurately the local radiant exposure in the region of the interferometer probe beam. This ambiguity was seen not to be a significant disadvantage since the analytic model can be used to estimate μ_a independently of radiant exposure. IR quartz attenuators were placed in the path of the Er:YSGG laser beam to adjust the local radiant exposure when necessary.

C. ArF Excimer Laser Irradiation of Bovine Corneal Stroma

The study was performed on bovine cornea *in vitro*. Calf eyes were employed to avoid any blemishes that may be found on mature bovine corneas and also to best mimic the geometry of human eyes. Although there are minor structural differences between bovine and human cornea, these differences are not thought to affect the spectroscopic characteristics or ablation dynamics of the cornea.[14]

An excimer laser (Lambda-Physik, Model LPX300) was used with an ArF gas fill (193-nm wavelength) to produce 600-mJ pulses of 20-ns duration (FWHM) at a repetition rate of 1 Hz. An aperture selected the central 4-mm disk of the 10 mm × 25 mm raw rectangular beam output. The beam energy was controlled with UV quartz attenuator plates of various thicknesses. A pyroelectric detector (Molectron Detector, Portland, Ore.) was used to measure the energy in each pulse. This was calibrated against a broadband pulse energy meter (Model J50, Molectron Detector). The experimental setup is depicted in Figs. 8 and 9. The plane of focus for the interferometer He–Ne beam served to define a fixed reference plane. The ArF beam was aligned to be concentric with the He–Ne probe at the reference plane. The transverse beam profile was measured in this plane by stepping a pyroelectric detector (Model J309, Molectron Detector) with a 1-mm-diameter aperture through the beam. The beam analysis permitted an estimate of the local radiant exposure for each laser pulse. The shot-to-shot energy variation of the ArF laser was less than 3%.

An acoustically thin barrier was employed to ensure that vaporization of cornea tissue constituents during the measurement did not interfere with the estimation of μ_a. Moreover the barrier helped guard against dehydration of the cornea. Borosilicate glass (type KG33, Kimble Glass) was used because it is easier to blow into a thin film than fused silica, is nearly transparent at 193 nm, and possesses a low thermal expansion coefficient ($\alpha_{T,\mathrm{KG33}} = 3.2 \times 10^{-6}$ 1/°C).[20] The glass was blown into spheres and shattered. The resulting 10-μm-thick shards of glass were draped over the bovine cornea like a contact lens. The laser pulse energy was not mechanically confined [$\tau_p \sim 20$ ns (FWHM) and $c_{a,\mathrm{KG33}} \sim 5640$ m/s (Ref. 20)] in the cornea. Thus the requirement for the glass membrane (b = 10 μm) to be acoustically thin $b \ll \tau_p c_{a,\mathrm{KG33}}/2$ is satisfied.

The radiant exposure measurement was adjusted for the expected reflection coefficient of 193-nm radiation incident at a 14° angle to air–glass incidence. The Fresnel reflectivity for both TE and TM reflection is ~5%, assuming that the refractive index of the glass is 1.55 at 193 nm. The reflectivity of the glass–cornea interface is negligible if the real part of the index of refraction for cornea is assumed to be 1.33 or higher [$n_{\mathrm{water}} = 1.33$ for visible light, $\mathrm{Re}(n_{\mathrm{cornea}})$ was measured to be 1.52 for 193-nm radiation[14]]. Thus

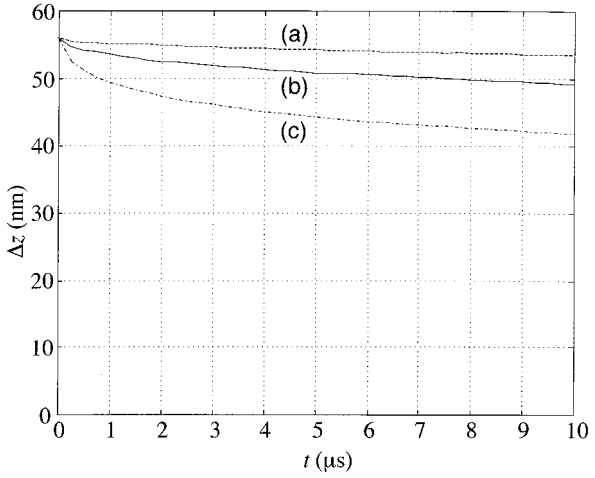

Fig. 10. $\Delta z(t)$ calculated for Q-switched Er:YSGG laser irradiation of water covered by an acoustically thin saran film. Note the sensitivity to μ_a for a fixed initial Δz. Traces are for (a) $\phi_0 = 765$ J/m^2 with $\mu_a = 2.3 \times 10^3$ cm^{-1}, (b) $\phi_0 = 650$ J/m^2 with $\mu_a = 4.6 \times 10^3$ cm^{-1}, (c) $\phi_0 = 535$ J/m^2 with $\mu_a = 9.2 \times 10^3$ cm^{-1}.

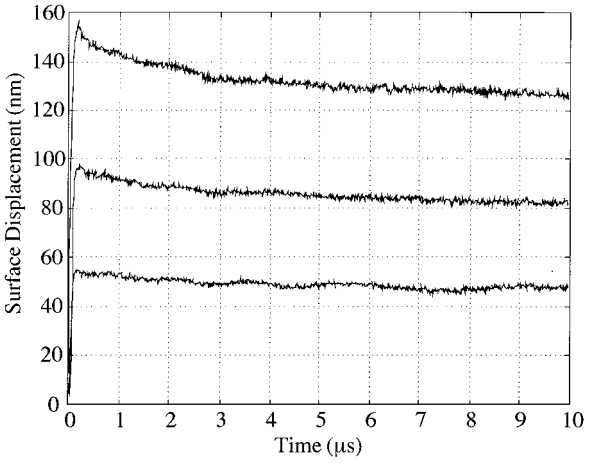

Fig. 11. Sample interferometer traces obtained for Q-switched Er:YSGG laser irradiation of saran-covered water at three different radiant exposures.

the glass membrane was not expected to result in Fabry–Perot interference of the 193-nm radiation, and multiple internal reflections need not be considered.

Whole bovine globes were obtained from a local slaughterhouse and used within 24 h. The globes were stored on ice and permitted to attain room temperature before the actual experiments. The epithelium covering the corneal stroma was removed by dragging a razor blade across the corneal surface, and the exposed stroma was wiped dry with lens tissue. A membrane of glass with an appropriate curvature was draped over the exposed stroma. The glass membranes were ~10 μm thick and ~5 mm across. Figure 9 contains an expanded view of the experimental setup. The globes were mounted in a three-axis positioning mount that permitted the glass-covered sections of cornea to be precisely positioned into the focal plane of the interferometer probe beam (hence the irradiation of the ArF beam). The heating of the cornea and the glass film by the He–Ne probe laser beam was ignored owing to the negligible absorption and scattering of glass and cornea at $\lambda = 632.8$ nm.

Displacement traces were acquired for several globes at a number of radiant exposure values. Many traces were acquired in the same conditions at the same site on the same cornea.

4. Results

A. Q-switched Er:YSGG Laser Irradiation of Water

Figure 10 depicts $\Delta z(t)$ predicted by the model for Q-switched Er:YSGG laser irradiation of a water substrate covered with 12.7-μm saran film at different radiant exposures ϕ_0 and absorption coefficients μ_a. Combinations of ϕ_0 and μ_a were chosen to give identical initial surface displacements. The water surface temperatures predicted by the model were 106, 72, and 51 °C for the 535-, 650-, and 756-J/m^2 traces, respectively. It is apparent from Fig. 10 that for a given initial surface displacement the temporal decay of Δz is sensitive to μ_a. The radiant exposure imparted by the laser was determined from the initial expansion. At the interferometer probe beam wavelength (632.8 nm) the refractive-index mismatch between the saran ($n = 1.6$) and the air ($n = 1$) resulted in a reflectivity of 5.3%, while the index mismatch between the saran film and the water ($n = 1.33$) resulted in a reflectivity of 2%. Thus the interferometer signal was reflected primarily from the saran–air interface. Three sample data traces are presented in Fig. 11. Note that for larger values of Δz at early times the temporal relaxation of Δz increases over the 10-μs trace. This occurs because the thermal expansion coefficient of water increases with increasing temperature. Thus a fixed amount of energy is conducted from the water into the saran film above it, and a higher initial temperature rise results in a larger downward surface displacement.

Note the presence of nanometer-scale microsecond-duration ripples in the traces. These ripples are presumably due to surface acoustic waves and may be a function of the smoothness of the laser transverse beam profile and the tautness of the saran film. We observed that the Gaussian transverse beam profile produced small ripples (like the ones depicted here), whereas an irregular transverse beam profile led to sufficient ripples to obscure the displacement relaxation.

A Levenberg–Marquardt nonlinear fitting algorithm (MATLAB, The Mathworks, Natick, Mass.) was employed to fit the model to 14 data traces by determination of the best value for μ_a and ϕ_0. This procedure was performed separately for each data trace, and thus 14 sets of μ_a and ϕ_0 were obtained. Approximately 1 min was required for convergence of the algorithm on an Apple PowerMac 7100/80 (Apple Computer, Cupertino, Calif.). The results of the algorithm were somewhat sensitive to the initial guess

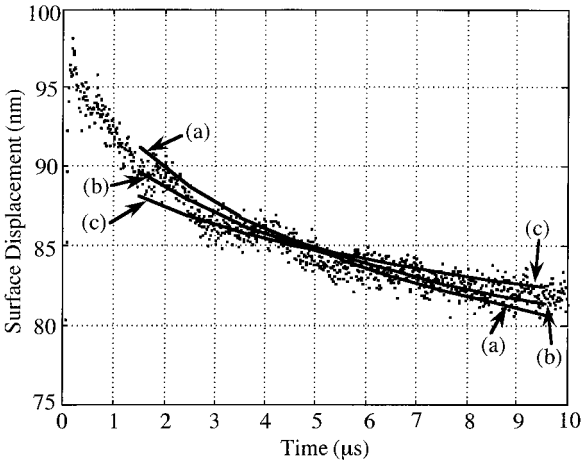

Fig. 12. Comparison between a measured single trace of surface displacement and a predicted Δz for three different combinations of μ_a and ϕ_0 (Er:YSGG laser irradiation of water sample): Trace (a) $\phi_0 = 923\ \mathrm{J/m^2}$, $\mu_a = 6.2 \times 10^3\ \mathrm{cm^{-1}}$; (b) $\phi_0 = 956\ \mathrm{J/m^2}$, $\mu_a = 5.0 \times 10^3\ \mathrm{cm^{-1}}$; (c) $\phi_0 = 1015\ \mathrm{J/m^2}$, $\mu_a = 3.7 \times 10^3\ \mathrm{cm^{-1}}$. The best-fit set of parameters for these measured data was found to be (b).

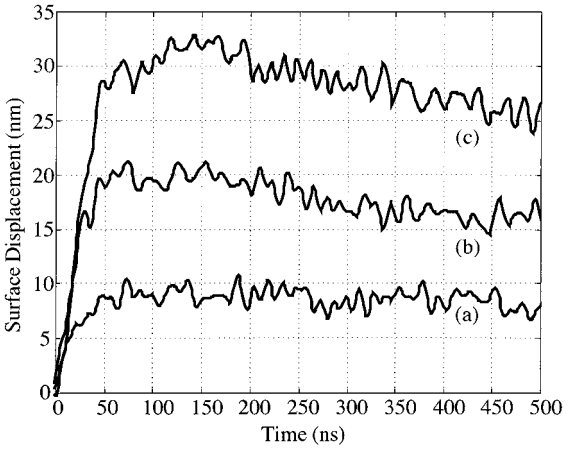

Fig. 13. Typical traces obtained by an interferometer for ArF excimer laser irradiation of a bovine corneal stroma covered by a glass membrane: (a) $\phi_0 = 156\ \mathrm{J/m^2}$, (b) $\phi_0 = 306\ \mathrm{J/m^2}$, (c) $\phi_0 = 364\ \mathrm{J/m^2}$.

for the radiant exposure. Thus a range of initial guesses covering the parameter space was employed to ensure that a global minimum was found. The chi-squared statistic was used to estimate the goodness of fit of the model for each trace, and based on this, several data traces were rejected.[21] The calculated radiant exposure values ϕ_0 corresponding to the individual surface-displacement traces ranged from 600 to 1100 $\mathrm{J/m^2}$. A single μ_a was computed based on the weighted average of the set of remaining μ_a values. The weighting for each value was based on the goodness of fit between the model and the data. Specifically, the inverse of the residuals was employed to weight each μ_a value. In this way μ_a was measured to be 5200 $\mathrm{cm^{-1}}$ with a weighted standard deviation of 500 $\mathrm{cm^{-1}}$. Assuming that the estimated values for μ_a are normally distributed, the 5–95% confidence interval for μ_a is approximately 4400–6000 $\mathrm{cm^{-1}}$. These results have taken into account the slight inclination of the Er:YSGG laser beam and thus represent our best estimate for the true value of μ_a. The expected range of μ_a based on published water spectra is 4610–5160 $\mathrm{cm^{-1}}$,[7,19] and this range of values lies well within the 5–95% confidence interval for our measurements.

In Fig. 12 a sample data trace is compared directly with model predictions given for three different combinations of μ_a and ϕ_0. For the sample data trace shown the best-fit parameter set was found to be $\phi_0 = 956\ \mathrm{J/m^2}$ and $\mu_a = 4950\ \mathrm{cm^{-1}}$. Note that fitting was performed from 1.5 to 9.5 μs after the end of the laser pulse. For comparison purposes, note that at $t = 5$ μs the model predicts the temperature at the saran–water interface to be 67, 73, and 79 °C for traces for which the absorption coefficient μ_a was set to 3.7, 5.0, and $6.2 \times 10^3\ \mathrm{cm^{-1}}$, respectively.

B. ArF Excimer Laser Irradiation of Bovine Corneal Stroma

Sample traces obtained by the interferometer for ArF excimer laser irradiation of bovine corneal stroma covered with a glass membrane are presented in Fig. 13. In Fig. 13 the time is measured with respect to the initiation of the upward motion of the surface displacement. Note that when the glass membrane covering the bovine cornea was removed following a series of measurements the covered area was slightly raised (by ~200 μm) relative to the uncovered corneal region. This was attributed to dehydration of areas of the cornea that remained exposed to ambient conditions over the course of the experiment.

The surface-displacement data traces acquired in the corneal tissue experiments were processed in a different manner compared with those acquired from the water experiments. In the water experiments 14 data traces were used independently to produce 14 different estimates for μ_a. A single estimate for μ_a and a confidence interval were computed from the set of estimates based on the residuals. However, the individual data traces acquired in the cornea experiments were too noisy to be independently used to generate an estimate for μ_a. Rather, many traces obtained at the same radiant exposure were averaged to generate a smoother single trace for a given radiant exposure. A confidence interval was determined by a Monte Carlo technique in which synthetic data sets with the same statistical characteristics as the actual data set were generated.[21] With this technique it is assumed that the individual data points were normally distributed around the true value with a characteristic error.

A nonlinear parameter fitting algorithm employing the Levenberg–Marquardt method (MATLAB, The Mathworks, Natick Mass.) was then employed to determine the best-fit values for ϕ_0 and μ_a. The ϕ_0 term was used as a fitting parameter even though it was measured during the experiment. This was

done since the fit between model and data is extremely sensitive to ϕ_0, and in practice it is nearly impossible to measure it accurately owing to the difficulty in measuring the transverse profile of the laser beam. Only traces obtained at the highest radiant exposures tested (>300 J/m^2) were used for estimating μ_a since traces at lower radiant exposures (<300 J/m^2) are much less sensitive to μ_a owing to the weaker nonlinearity in the dependence of water density on temperature. To generate model predictions for the fitting procedure, it was necessary to know the thermophysical properties for the corneal stroma. Unfortunately, they are not well tabulated in the literature, and most authors (see, for example, Refs. 22–24) have assumed values similar to those of water owing to the high water content of the stroma (78% by mass). For this reason the thermophysical properties of cornea were assumed to be equivalent to those of water for this study.

The nonlinear fitting procedure yielded the value μ_a = 19,400 cm^{-1} (D = 515 nm). This result takes into account the slight inclination of the ArF excimer laser pump beam, and so it represents our best estimate for the true value of μ_a. Approximately 1 min of computation time was required for convergence of the algorithm as was the case for the Er:YSGG laser experiments described above. The results of the nonlinear fitting algorithm were somewhat dependent on the initial guess for the radiant exposure, so many initial guesses covering the parameter space were employed to ensure that the true best fit to the data was found. The chi-squared statistic was employed to demonstrate the goodness of fit between the model and the data.[21] The resulting 5–95% confidence interval for μ_a determined from using the synthetic data set was 16,000–23,000 cm^{-1} (D = 435–633 nm). The ArF laser radiant exposure was measured to be approximately 390 J/m^2, whereas the nonlinear fitting procedure determined it to be approximately 340 J/m^2. The 15% difference between measured and calculated radiant exposure is consistent with the characteristic experimental uncertainty in measuring this quantity.

The averaged data trace used for the μ_a estimation is presented in Fig. 14 along with predicted traces for a few combinations of μ_a and ϕ_0. The values for μ_a depicted in the plot include μ_a = 2700 cm^{-1} measured by Puliafito and co-workers,[8] μ_a = 39,900 cm^{-1} measured by Pettit and Ediger,[14] and the best-fit value found in this study. The values from the literature clearly do not fit the data as well as 19,400 cm^{-1}. For comparison purposes the cornea–glass interface temperatures predicted by the model at t = 350 ns were 34, 75, and 96 °C for traces with μ_a equal to 2700, 19,400, and 39,900 cm^{-1}, respectively.

To examine the displacement dynamics at early times, (<150 ns), Eqs. (1) and (2) were implemented numerically with the FEM (MATLAB, The Mathworks). An analytic function was fitted to the temporal profile of the ArF excimer laser pulse as measured by a single-nanosecond rise-time detector (Model P5-01, Molectron Detector) and was used for the FEM solution. The FEM solution was not used with the Levenberg–Marquardt fitting algorithm since it required excessive computation time. In Fig. 15 the FEM solution with the best-fit parameters for μ_a and ϕ_0 is compared with the measured data. A significant discrepancy is apparent at times earlier than 100 ns after the start of the laser pulse. In contrast to the data the best-fit model reaches its maximum surface displacement at the conclusion of the laser pulse, 50 ns after it began. The measured data trace lags behind and achieves its maximum surface displacement at around 100 ns from the start of the laser pulse. The maximum temperature predicted by the FEM solution is 121 °C at z = 126 nm and t = 52 ns. The presence of tissue water in a metastable state

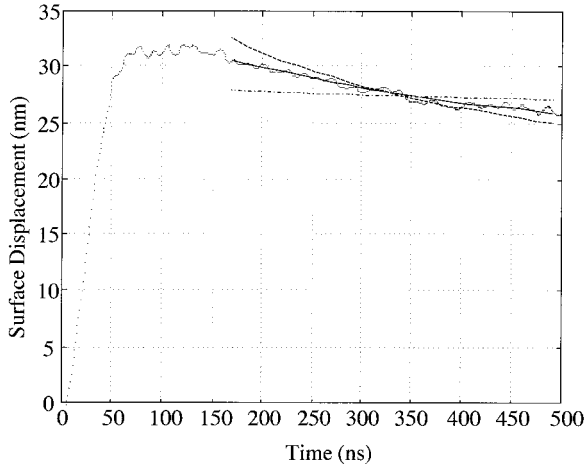

Fig. 14. Comparison between an averaged data trace (dotted curve) obtained for pulsed ArF excimer irradiation of bovine cornea and the best fit of a model when three different sets of μ_a and ϕ_0 are used. Dashed curve, best fit obtained with the absorption coefficient cited by Pettit and Ediger[14] (ϕ_0 = 333 J/m^2, μ_a = 4 × 10^4 cm^{-1}); dash–dot curve, best fit obtained with the absorption coefficient cited by Puliafito *et al.*[8] (ϕ_0 = 435 J/m^2, μ_a = 2.7 × 10^3 cm^{-1}), solid curve, overall best fit (ϕ_0 = 338 J/m^2, μ_a = 1.9 × 10^4 cm^{-1}).

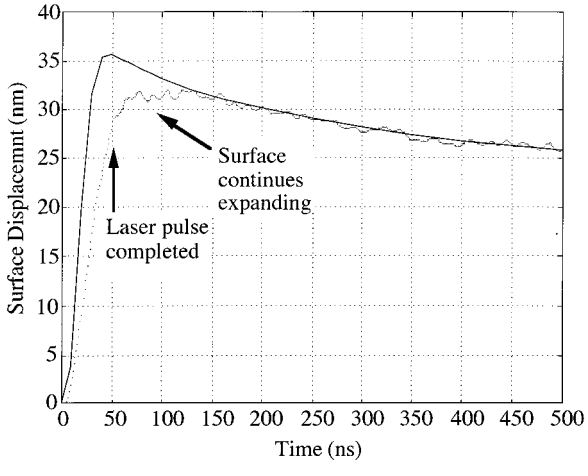

Fig. 15. Comparison between the averaged data trace obtained for pulsed ArF excimer irradiation of bovine cornea (dotted curve) and the best-fit FEM model (solid curve). For the best-fit FEM model, μ_a = 1.9 × 10^4 cm^{-1} and ϕ_0 = 338 J/m^2.

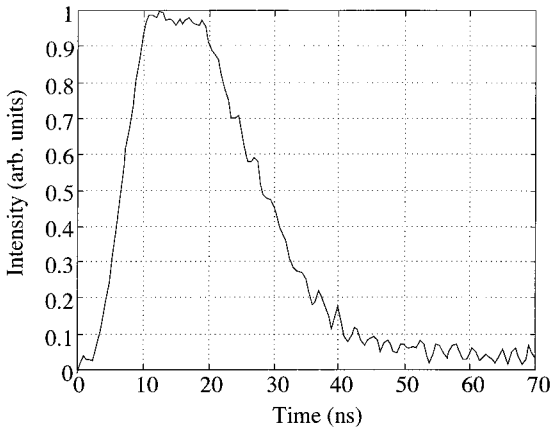

Fig. 16. ArF excimer laser pulse temporal profile.

should not disturb the reader since this situation persists for only a few tens of nanoseconds, and moreover Eq. (8) is valid to as high as 150 °C.

For comparison purposes the temporal profile of the ArF excimer laser pulse is presented in Fig. 16. Note that the weak tail of energy following the laser pulse is not sufficient to account for the discrepancy. Moreover the discrepancy cannot be resolved by invoking nonlinear absorption behavior that would lead to a nonexponential spatial energy deposition profile. Aside from the possibility that the corneal stroma has thermal expansion characteristics that are different from water, the only other explanation for the discrepancy at early times is that some of the laser pulse energy is not fully thermalized in the water until 100 ns after the termination of the laser pulse.

5. Discussion

The agreement between the IPTS-measured absorption coefficient of pure water at 2.79 μm and the values in the literature suggests that under the proper conditions IPTS is a valid technique for absorption coefficient measurement. It is impressive that across a large range of radiant exposure (600–1100 J/m^2) the individual estimates for μ_a had a relative standard deviation of approximately 10%. The fact that the μ_a values obtained from the various traces agreed with one another indicates that the model is a correct description of the dynamics of Er:YSGG laser irradiation of tissue and can be used to estimate μ_a for similar laser–tissue interactions. Soft biological tissues, such as corneal stroma, are primarily water, and consequently it is reasonable to infer that the IPTS technique is capable of accurately estimating the absorption coefficients of such tissues.

Several potentially important effects are ignored in our model for ArF excimer laser irradiation of corneal stroma. First, as mentioned above, the thermophysical properties of corneal stroma are not known and moreover are likely to vary with temperature. Owing to the high water content of corneal stroma, the thermophysical properties were assumed to be equivalent to those of water. The corneal stroma was treated as a liquid with a Poisson's ratio of 0.5 in Eq. (7), since the temperature-driven volume-expansion properties of water were expected to dominate any effects resulting from the anisotropic collagen matrix.[24] The structure of the cornea suggests that there may be heterogeneities on the same spatial scale as the measured absorption depth since the individual collagen lamellae are said to be approximately 2 μm thick.[25] However, if the structure of the lamellae is such that the relative concentrations of collagen and water do not vary on the scale of laser penetration, the influence of this heterogeneity would be negligible.

Experiments have shown that the hydration state of the cornea has a significant effect on its absorption characteristics at 193 nm and that the absorption has a time-varying behavior.[9–11] In this study care was taken to ensure that the hydration state of the cornea was maintained at its proper physiological level. Indeed it appeared that the glass membrane inhibited desiccation of the cornea surface on the time scale necessary to perform a set of measurements on a single eye (~20 min). After a set of measurements was completed, the areas covered by the glass membrane were approximately 200 μm higher than the exposed area, indicating significant dehydration of the uncovered areas.

We neither considered nor observed the effects of repetitive exposure of a single site, most likely because we employed strictly subablative exposures for our measurements and because no incubation effect has been documented for 193-nm irradiation of the cornea.[26]

Note the extremely small vertical scale in Fig. 13 and the noise level of ±1 nm. Providing $D \ll 30$ μm (which seems assured given the range of published values for this parameter[8–11,13,14]), the 20-ns FWHM ArF excimer laser pulse is not mechanically confined. The rise time of the lower traces corresponds to the 20-ns FWHM duration of the ArF laser pulse and is a consequence of the lack of mechanical confinement of the laser pulse, which permits thermal expansion on the time scale of the irradiation. As in Fig. 11 the amount of downward surface relaxation increases with increasing radiant exposure. This is not surprising since, for a fixed amount of energy conducted from the heated corneal stroma into the glass membrane, more surface motion is expected at higher temperatures owing to the nonlinear dependence of water density on temperature. The time scale for relaxation is much faster in these traces compared with those in Fig. 11 and is indicative of a more shallow penetration depth (higher μ_a).

The model can be fitted to the data only over a finite time interval. The model assumes an instantaneous energy deposition and consequently is not expected to agree with the data during and immediately after irradiation (i.e., for $t < 150$ ns). For times longer than 500 ns after laser irradiation, significant acoustic effects corrupted the data traces; therefore only the first 500 ns of the data traces were suitable for μ_a estimation. This is not surprising since the bovine corneal stroma is only ~0.4 mm thick. Conse-

quently it does not take much longer than 500 ns for an acoustic wave to travel from the front side of the cornea to the rear side and return again to the front side if $c_{a,\text{cornea}} \sim 1500$ m/s is assumed.

Pettit and Ediger[14] provide evidence that the value for μ_a cited by Puliafito *et al.*[8] is likely to have been corrupted by problems with sample preparation. Pettit and Ediger also documented how the existence of a thin water layer between the prism and the cornea in their experimental apparatus may have led them to overestimate μ_a (and underestimate D).[14] The water layer might have resulted from pressure applied on the cornea by the prism. In unpublished experiments we have observed that pressure applied to the corneal stroma indeed caused it to sweat significant amounts of moisture, perhaps in the same manner that a sponge surrenders moisture when compressed. Consequently one reason for the discrepancy between the value for μ_a measured here and that cited by Pettit and Ediger[14] may be the formation of a pressure-induced water layer in their experimental apparatus. Clearly, further investigation is needed to resolve these differences.

The IPTS measurement of μ_a was done near ablation-threshold radiant exposures as opposed to the measurements of Pettit and Ediger[14] that were done at very low radiant exposures. It is possible that μ_a depends on the local energy density, as has been demonstrated for Er:YAG laser irradiation of water.[7,27] If so, reconciling the measurements here with those of Pettit and Ediger[14] would require that μ_a decrease with increasing local energy density. However, this conflicts with a recent study indicating that μ_a is expected to increase with increasing local energy density.[12]

The value of the absorption coefficient μ_a is critical to understanding the dynamics of ArF excimer laser ablation of corneal tissue since this parameter determines how the laser energy is deposited. Currently there is some debate in the literature concerning whether the ablation process is solely thermal or is in part driven by photochemical processes. Srinivasan and co-workers[13,28,29] have proposed that corneal ablation proceeds through ablative photodecomposition as has been demonstrated for ArF excimer laser ablation of organic polymers. Their hypothesis is that the collagen matrix in the cornea is photochemically decomposed into smaller molecular fragments by the high-energy (6.4-eV) 193-nm photons. The higher specific volume and high kinetic energy of these fragments are said to drive the material-removal process.

The surface-displacement model presented in this paper assumes that all the energy imparted by the laser pulse is thermalized. A comparison between the FEM solution and the measured data (Fig. 15) suggests that for times of less than 150 ns after the laser pulse the energy may not be thermalized because the cornea continues to expand after the laser pulse has ceased and thermal stresses are presumed to have equilibrated. However, for times of more than 150 ns after the start of the laser pulse the excellent fit between model and data suggests that the pulse energy is fully thermalized. One possible explanation is that the thermal expansion of collagen, which is the site of absorption, is small and that the absorbed energy requires many nanoseconds to be transferred to the bound and free water that has a much greater thermal expansion and also comprises most of the corneal tissue mass. Another possible explanation is that some of the pulse energy manifests itself chemically rather than thermally at times of less than 150 ns after the laser pulse. Other researchers have noted that ablation characteristics at the fifth harmonic of the Nd:YAG laser (213 nm) are similar to those at 193 nm.[12,30–32] It would be interesting to repeat the measurements here with 213-nm irradiation to determine whether the resulting surface-displacement dynamics possess similar characteristics.

Since the interferometer tracks the motion of a surface in an epitaxial manner (accessing the surface from one side only) the method may be readily employed on living tissue. There is nothing that prevents the implementation of such an interferometer by use of optical fibers that can be passed through an endoscope or a laparoscope to measure μ_a deep inside a living patient. Such measurements could be of diagnostic value because they could conceivably gauge the state of a tissue. However, IPTS requires that the absorption coefficients being measured be approximately 10^3–10^5 cm^{-1} when employed for soft biological tissue.

Equations (4)–(8) are nonlinear; so it appears to be impossible to invert these equations to yield a model that will explicitly provide μ_a given a surface-displacement trace measured by the interferometer. The alternative is to execute a nonlinear parameter fitting algorithm, such as the Levenberg–Marquardt method, to estimate both the radiant exposure ϕ_0 and the absorption coefficient μ_a given a measured displacement trace. If μ_a is well characterized, the model derived here can be combined with measured displacement traces to measure other thermophysical properties appearing in the derivation. For example, if α_1, the thermal diffusivity of the target material, is desired, one can use a Levenberg–Marquardt fitting algorithm to find the value that yields a best fit between the model and the data.

IPTS may also prove useful for nondestructive evaluation of thin films or laminates. The optical properties of thin-film semiconductor coatings may be readily assessed with this technique. Alternatively, if the absorption coefficient of the material is well known, the same equipment and modeling employed for IPTS can be used to obtain the thermophysical properties of the material.

5. Conclusions

IPTS is a novel technique for measuring the absorption coefficient of a short laser pulse in tissue. It can be used to obtain estimates of the tissue absorption coefficient in situations in which other techniques fail, such as pulsed ArF excimer laser irradiation (193 nm) of corneal stroma. When IPTS was used, the absorption coefficient of cornea was determined to be

19,000 ± 4000 cm^{-1}. A comparison between the model and the measured displacement traces during ArF excimer laser irradiation of corneal stroma suggests that many nanoseconds are required for the complete thermalization of the laser pulse energy in the corneal water. This may be due to the transfer of thermal energy from the corneal collagen to the free water or to some of the laser pulse energy being manifested as chemical energy. Further research is needed to determine the reason for the observed dynamics.

Since it is epitaxial and requires minimal perturbation of the tissue sample, IPTS may have applications as a minimally invasive diagnostic for an *in vivo* estimation of the optical penetration depth of a laser pulse. In future research this potential should be explored.

Appendix A

Here we derive Eq. (7), which describes thermal expansion for isotropic incompressible materials that are constrained to expand in one direction only. In this derivation the elastic properties (elastic modulus E, Poisson's ratio ν) are treated as constants, whereas the density of the material is permitted to be a nonlinear function of temperature (i.e., the thermal-expansion coefficient α_T may vary with temperature). In cases in which the assumptions in this derivation are too restrictive, the thermoelastic behavior of the tissue can always be treated numerically.

In our orthogonal coordinate system a thermally expanding body occupies the half-space $z > 0$. The net thermal expansion of this body is given by Δz:

$$\Delta z = \int_0^\infty \varepsilon_{zz} \mathrm{d}z, \tag{A1}$$

where ε_{zz} is the strain in the z direction (negative for compressive strain). In general ε_{zz} may be a function of time t, so Δz may also be a function of time. The symmetry of the problem and the fact that the temperature field is assumed to be a function of only z and t demand that there be no displacements in the x or the y direction:

$$u_x = 0, \qquad u_y = 0, \qquad u_z = u_z(z). \tag{A2}$$

The strain tensor ε_{ij} may be expressed as[33]

$$\varepsilon_{ij} = \tfrac{1}{2}(u_{i,j} + u_{j,i}), \tag{A3}$$

which in our case reduces to

$$\varepsilon_{zz} = \frac{\partial u_z}{\partial z} \tag{A4}$$

with all other $\varepsilon_{ij} = 0$.

In a linear elastic isotropic body the relation between stress and strain may be written as

$$\varepsilon_{ij} = \frac{1+\nu}{E}\sigma_{ij} - \frac{\nu}{E}\sigma_{kk}\delta_{ij} + \frac{\Delta V}{3V}\delta_{ij}, \tag{A5}$$

where σ_{ij} is the stress tensor (negative for compression), δ_{ij} is Kronecker's delta, ν is Poisson's ratio, and E is the elastic modulus. This expression differs from that of Timoshenko and Goodier[33] in that $\Delta V/3V$ is used in place of $\alpha_T \Delta T$. $\Delta V/V$ is the fractional volume change (pure dilatation) that would result from a temperature change in the absence of stress. Note that, for a material with a constant thermal-expansion coefficient α_T, $\Delta V/3V = \alpha_T \Delta T$, where ΔT is the local temperature change.

Owing to symmetry, the normal strain in the x direction σ_{xx} is equal to the normal strain in the y direction σ_{yy}, and consequently we denote both of them by $\sigma_\perp$. Since there are no shear strains there can be no shear stresses. Equation (A5) reduces to

$$\varepsilon_{zz} = \frac{\sigma_{zz}}{E} - \frac{2\nu\sigma_\perp}{E} + \frac{\Delta V}{3V},$$

$$0 = \frac{(1-\nu)\sigma_\perp}{E} - \frac{\nu\sigma_{zz}}{E} + \frac{\Delta V}{3V}. \tag{A6}$$

Assuming that the stresses have equilibrated in the z direction so that $\sigma_{zz} = 0$, $\sigma_\perp$ may be algebraically eliminated to yield

$$\varepsilon_{zz} = \left(\frac{1+\nu}{1-\nu}\right)\frac{\Delta V}{3V}. \tag{A7}$$

Equation (A7) expresses the strain in the z direction as a function of the stress in the z direction and the local free thermal expansion. This general expression can be used in Eq. (A1) to find the net thermal expansion in the z direction.

One can express $\Delta V/V$ as a function of temperature providing the temperature dependence of the density is well characterized. The net volume change ΔV of a cube with edge length L is given by

$$\Delta V = (L + \Delta L)^3 - L^3, \tag{A8}$$

where ΔL is the change in length of the cube edge. If ΔL is small compared with L, higher-order terms can be neglected, and the fractional volume change may be written as

$$\frac{\Delta V}{V} = 3\,\frac{\Delta L}{L}. \tag{A9}$$

The mass of the cube does not change with the dilatation and is given by its density times its volume. Consequently

$$\rho_0 L^3 = \rho_1 (L + \Delta L)^3 \approx \rho_1 (L^3 + 3L^2 \Delta L), \tag{A10}$$

where $\approx$ indicates that higher-order terms have been neglected. Expression (A10) can be manipulated to yield

$$3\,\frac{\Delta L}{L} = \left(\frac{\rho_0}{\rho_1} - 1\right). \tag{A11}$$

Equations (A9) and (A11) may be substituted into Eq. (A7) to yield the strain in the z direction:

$$\varepsilon_{zz} = \frac{1}{3}\left(\frac{1+\nu}{1-\nu}\right)\left\{\frac{\rho_0}{\rho[T(z,t)]} - 1\right\}. \tag{A12}$$

This is the general expression for the strain encountered during IPTS, and it may be used as the integrand in Eq. (A1) for any linear elastic isotropic material. Samples of pure water are assumed to be nearly incompressible; so ν is taken to be 0.5 and Eq. (A1) may be written as

$$\Delta z(t) = \int_0^\infty \left\{ \frac{\rho_0}{\rho[T(z, t)]} - 1 \right\} dz. \qquad \text{(A13)}$$

Equation (A13) is identical to Eq. (7) when coordinate z is replaced with z_0. Equation (A13) is also valid for IPTS measurements of corneal tissue since, despite its structural anisotropy, the cornea has been measured to be nearly incompressible ($\nu \sim 0.48$) since it is $\sim$80% water.[24]

The authors thank Barry Payne, Robert Webb, and Thomas Deutsch for advice and technical assistance. This research was made possible by the Whitaker Foundation, U.S. Army grant USAMRDC-DAMD17-94-C-4009, Augmentation Awards for Science and Engineering Research grant ONR-DAAH04-95-1-0216, and the Laser Microbeam and Medical Program resource RR01192 supported by the National Institute of Health.

Address correspondence to V. Venugopalan, Laser Microbeam and Medical Program, Beckman Laser Institute, 1002 Health Sciences Rd., University of California, Irvine, Irvine, CA 92612.

References

1. S. A. Prahl, I. A. Vitkin, U. Bruggemann, B. C. Wilson, and R. R. Anderson, "Determination of optical properties of turbid media using pulsed photothermal radiometry," Phys. Med. Biol. **37,** 1203–1217 (1992).
2. T. E. Milner, D. J. Smithies, D. M. Goodman, A. Lau, and J. S. Nelson, "Depth determination of chromophore in human skin by pulsed photothermal radiometry," Appl. Opt. **35,** 3379–3385 (1996).
3. I. Itzkan, D. Albagli, M. L. Dark, L. T. Perelman, C. von Rosenberg, and M. S. Feld, "The thermoelastic basis of short pulsed laser ablation of biological tissue," Proc. Natl. Acad. Sci. **92,** 1960–1964 (1995).
4. D. Albagli, M. L. Dark, L. T. Perelman, C. von Rosenberg, I. Itzkan, and M. S. Feld, "Photomechanical basis of laser ablation of biological tissue," Opt. Lett. **19,** 1684–1686 (1994).
5. D. Albagli, "Fundamental mechanisms of pulsed laser ablation of biological tissue," Ph.D. dissertation (Massachusetts Institute of Technology, Cambridge, Mass., 1994).
6. J. T. Walsh, Jr., and J. P. Cummings, "Effect of the dynamic optical properties of water on mid-infrared laser ablation," Lasers Surg. Med. **15,** 295–305 (1994).
7. K. L. Vodopyanov, "Saturation studies of H_2O and HDO near 3400 cm^{-1} using intense picosecond laser pulses," J. Chem. Phys. **94,** 5389–5393 (1991).
8. C. A. Puliafito, R. F. Steinert, T. F. Deutsch, F. Hillenkamp, E. J. Dehm, and C. M. Adler, "Excimer laser ablation of the cornea and lens," Ophthalmology **92,** 741–748 (1985).
9. M. N. Ediger, G. H. Pettit, R. P. Weiblinger, and C. H. Chen, "Transmission of corneal collagen during ArF excimer laser ablation," Lasers Surg. Med. **13,** 204–210 (1993).
10. M. N. Ediger, G. H. Pettit, and D. W. Hahn, "Enhanced ArF laser absorption in a collagen target under ablative conditions," Lasers Surg. Med. **15,** 107–111 (1994).
11. G. H. Pettit, M. N. Ediger, and R. P. Weiblinger, "Dynamic optical properties of collagen-based tissue during ArF excimer laser ablation," Appl. Opt. **32,** 488–492 (1993).
12. P. T. Staveteig and J. T. Walsh, Jr., "Dynamic 193-nm optical properties of water," Appl. Opt. **35,** 3392–3403 (1996).
13. R. Srinivasan, P. E. Dyer, and B. Braren, "Far-ultraviolet laser ablation of the cornea: photoacoustic studies," Lasers Surg. Med. **6,** 514–519 (1987).
14. G. H. Pettit and M. N. Ediger, "Corneal-tissue absorption coefficients for 193- and 213-nm ultraviolet radiation," Appl. Opt. **35,** 3386–3391 (1996).
15. E. M. Sparrow and R. D. Cess, *Radiation Heat Transfer*, Augmented ed. (Brooks/Cole, Belmont, Calif., 1978).
16. R. C. Weast, *CRC Handbook of Chemistry and Physics* (CRC Press, Boca Raton, Fla., 1987).
17. A. D. Yablon, N. S. Nishioka, B. B. Mikic, and V. Venugopalan, "An interferometer for monitoring the surface displacement of a reflecting biological tissue surface," in *Advances in Heat and Mass Transfer in Biotechnology*, HTD-337/BED-34, L. J. Hayes and S. Clegg, eds. (American Society of Mechanical Engineers, New York, 1996), pp. 75–80.
18. Dow Chemical Corporation, Typical properties for Saran Wrap 19, Product data sheet 190-00456-496RJD (Dow Chemical Corporation, Midland, Mich., 1997).
19. H. D. Downing and D. Williams, "Optical constants of water in the infrared," J. Geophys. Res. **80,** 1656–1661 (1975).
20. Kimble Glass Corporation, Properties of Kimble Glasses, Product data sheet (Kimble Glass Corporation, Vineland, N.J., 1997).
21. W. H. Press, B. P. Flannery, S. A. Teukolsky, and W. T. Vetterling, *Numerical Recipes in C* (Cambridge University, New York, 1988).
22. A. F. Emery, P. Kramar, A. W. Guy, and J. C. Lin, "Microwave induced temperature rises in rabbit eyes in cataract research," J. Heat Transfer **97,** 123–128 (1975).
23. J. A. Scott, "A finite element model of heat transport in the human eye," Phys. Med. Biol. **33,** 227–241 (1988).
24. J. L. Battaglioli and R. D. Kamm, "Measurements of the compressive properties of scleral tissue," Invest. Ophthalmol. Vis. Sci. **25,** 59–65 (1984).
25. D. M. Maurice, "The cornea and sclera," in *The Eye*, H. Davson, ed. (Academic, New York, 1984), Vol. 1b, pp. 1–158.
26. G. H. Pettit, M. N. Ediger, and R. P. Weiblinger, "Excimer laser corneal ablation: absence of a significant 'incubation' effect," Lasers Surg. Med. **11,** 411–418 (1991).
27. J. P. Cummings and J. T. Walsh, Jr., "Erbium laser ablation: the effect of dynamic optical properties," Appl. Phys. Lett. **62,** 1988–1990 (1993).
28. B. J. Garrison and R. Srinivasan, "Laser ablation of organic polymers: microscopic models for photochemical and thermal processes," J. Appl. Phys. **57,** 2909–2914 (1985).
29. R. Srinivasan and B. Braren, "Ultraviolet laser ablation of organic polymers," Chem. Rev. **89,** 1303–1316 (1989).
30. Q. Ren, R. P. Gailitis, K. P. Thompson, and J. T. Lin, "Ablation of the cornea and synthetic polymers using a UV (213 nm) solid-state laser," IEEE J. Quantum Electron. **26,** 2284–2288 (1990).
31. Q. Ren, G. Simon, J.-M. Legeais, J.-M. Parel, W. Culbertson, J. Shen, Y. Takesue, and M. Savoldelli, "Ultraviolet solid-state laser (213-nm) photorefractive keratectomy," Ophtalmology **101,** 883–889 (1994).
32. Q. Ren, R. H. Keates, R. A. Hill, and M. W. Berns, "Laser refractive surgery: a review and current status," Opt. Eng. **34,** 642–658 (1995).
33. S. P. Timoshenko and J. N. Goodier, *Theory of Elasticity*, 3rd ed. (McGraw-Hill, New York, 1970).